International Journal of Geo-Engineering

RESEARCH Open Access

A comparative analysis of laboratory, in-situ, and observational methods for predicting the magnitude and duration of consolidation settlement: Northern Marmara highway case history

Alparslan Doğan[1*] and Sami Oguzhan Akbaş[1]

*Correspondence:
Alparslan Doğan
alparslan.dogan@gazi.edu.tr
[1]Department of Civil Engineering, Faculty of Engineering, Gazi University, Ankara, Türkiye

Abstract

Accurate prediction of both the magnitude and the time rate of consolidation settlement remains challenging in layered soft soils because key inputs—stress history (OCR), primary consolidation-rate parameter (c_v), and the effective drainage distance (d)—are often uncertain and are commonly evaluated using laboratory tests, in-situ indices, or settlement records in isolation. This study presents a case-history comparison of these approaches using comprehensive site investigations and settlement monitoring from the Northern Marmara Highway (NMH/KMO) embankment. Preconsolidation pressure/OCR profiles were derived from laboratory consolidation curves and evaluated against independent field evidence using CPT- and SPT-based correlations; these OCR trends were then used in one-dimensional settlement calculations, including an additional stratified scenario in which drainage-competent sandy/silty strata were excluded from the compressible clay thickness based on CPT soil classification. For time-rate assessment, laboratory-based and CPT-dissipation-based c_v were evaluated together with a liquid-limit-based range drawn from NAVFAC guidance, and the monitored settlement–time records were analysed using multiple observational fitting methods. The results show that settlement predictions are highly sensitive to OCR interpretation and drainage-distance assumptions in stratified deposits. When CPT-based drainage boundaries are incorporated into the interpretation of dissipation-derived in-situ indices, the resulting settlement–time predictions align with the monitored response. The study provides a practical basis for reconciling laboratory, in-situ, and monitoring-based inputs when assessing primary consolidation settlement in layered soils.

Keywords Consolidation settlement, Overconsolidation ratio (OCR), Coefficient of consolidation (c_v), CPT dissipation, Drainage distance, Observational methods

© The Author(s) 2026. **Open Access** This article is licensed under a Creative Commons Attribution 4.0 International License, which permits use, sharing, adaptation, distribution and reproduction in any medium or format, as long as you give appropriate credit to the original author(s) and the source, provide a link to the Creative Commons licence, and indicate if changes were made. The images or other third party material in this article are included in the article's Creative Commons licence, unless indicated otherwise in a credit line to the material. If material is not included in the article's Creative Commons licence and your intended use is not permitted by statutory regulation or exceeds the permitted use, you will need to obtain permission directly from the copyright holder. To view a copy of this licence, visit http://creativecommons.org/licenses/by/4.0/.

Introduction

Designing embankments on soft, stratified deposits requires reliable predictions of both the ultimate primary consolidation settlement and its development with time. In routine practice, the settlement–time response is still commonly evaluated using Terzaghi's one-dimensional formulation, which is governed by stress history (σ'_p/OCR), coefficient of consolidation (c_v), and an effective drainage path (d). In thick layered profiles, these inputs are often imperfectly constrained: stress history can vary with depth and drainage boundary conditions may be uncertain; therefore, although a single representative c_v is adopted for design, its selection should be made cautiously, acknowledging the stress and stratification dependent coupling between compressibility and permeability. Because c_v is a derived parameter rather than a material constant, its value is only meaningful when paired with a compatible OCR interpretation and an explicitly defined drainage path. Case histories show that adopting constant c_v together with simplified drainage assumptions can bias time-rate estimates, particularly when stratigraphic idealization and drainage boundaries are uncertain Leroueil and Tavenas [39].

In consolidation settlement assessment, designers commonly draw on both laboratory oedometer tests and field evidence, and the two do not always converge. Laboratory c_v is sensitive to specimen quality, sampling disturbance, and test execution [16, 30]. Comparative studies show that laboratory- and field-derived c_v can differ substantially; as a result, predicted consolidation time can vary markedly with the adopted basis for c_v unless it is constrained by the observed settlement–time response [25].

To infer c_v from in-situ response, piezocone dissipation tests are widely used; however, the inferred c_v depends on the adopted interpretation framework and its idealized boundary conditions [5, 23, 32]. In stratified deposits, dissipation therefore tends to define a depth-dependent range of c_v, rather than a unique constant. LL-based guidance can also be used as a practical screening reference, provided that the selected trend is consistent with stress history [19]. In this study, stress history (σ'_p/OCR) is established first and used to select the LL-based trend and to screen dissipation- and laboratory-derived c_v estimates before confronting them with the monitoring-derived settlement–time behaviour.

Recent studies in subgrade-focused contexts have advanced field-test-based indices for rapid characterization of strength and stiffness using portable in-situ devices [13, 14]. Direct settlement–field-test comparisons have also been reported in earthwork settings where surface deformation can be monitored or inferred and juxtaposed with penetration-based indicators [15]. For consolidation settlement in stratified soft clays, however, uncertainty in the time scale is often strongly influenced by the effective drainage distance implied by stratigraphy. Drainage-competent bands (e.g., silt or sand seams) can shorten the effective drainage path; unless such layers are identified and explicitly represented in the drainage model, settlement–time predictions can span a wide range under otherwise reasonable c_v values. CPT dissipation tests have been used in instrumented embankment case histories to estimate consolidation parameters and compare predicted settlement evolution against monitoring records; nevertheless, the settlement–field-test evidence base for consolidation time-rate remains largely case-history based, limiting calibration and generalisation beyond a small number of well-documented sites [1, 2].

This study addresses these practical gaps using the Northern Marmara Highway (NMH/KMO) embankment case history. Within the same dataset, (i) σ'_p/OCR

uncertainty is explicitly addressed by benchmarking σ'_p/OCR from laboratory interpretations [7 24] methods) against CPT/SPT correlations and propagating OCR trends into settlement computations; (ii) drainage distance is treated as an explicit, test-supported modelling choice by inferring drainage-competent layers from CPT soil behaviour type (SBT) profiles; (iii) c_v values from laboratory oedometer tests are compared with CPT dissipation and with LL-based NAVFAC [19] ranges as an independent reference; and (iv) the monitoring records are analysed with multiple observational formulations to examine fitting-window sensitivity and robustness.

Case history

Project and embankment description

The Northern Marmara Highway (NMH; KMO in Turkish) project was delivered under a Build–Operate–Transfer (BOT) model and comprises three main sections—Kınalı–Odayeri, Odayeri–Paşaköy, and Kurtköy–Akyazı—subdivided into seven subsections, as shown in Fig. 1. The study site is located within Subsection 6 of the Kurtköy–Akyazı main section, near project chainage Km 241 + 400, in the vicinity of the Mudurnu River crossing where Bridge K26 is situated (Fig. 2). The bridge approach embankment, with a 45 m crest width and 2 H:1 V side slopes, was constructed in stages over approximately 5–7 days, reaching a maximum height of 5.5 m.

Figure 3 presents a 3D geological model together with a unified topographic map of the region. The plain hosting the embankment was formed primarily by fluvial processes associated with the Sakarya and Mudurnu Rivers, which have governed the depositional environment and, consequently, the soil-profile development across the study area [37]. The Sakarya Plain extends from Lake Sapanca to the town of Akyazı. As illustrated in the figure, the accumulation of thick alluvial deposits reaches up to 300 m in depth at the central section of the plain [4].

Subsurface conditions and geotechnical characterization

The locations of exploratory borings and CPTs planned by the geotechnical design consultant are shown in Fig. 4, and a list of available in-situ tests is provided in Table 1.



Fig. 1 Plan view of the NMH/KMO project



Fig. 2 Satellite view of the embankment and K26 bridge

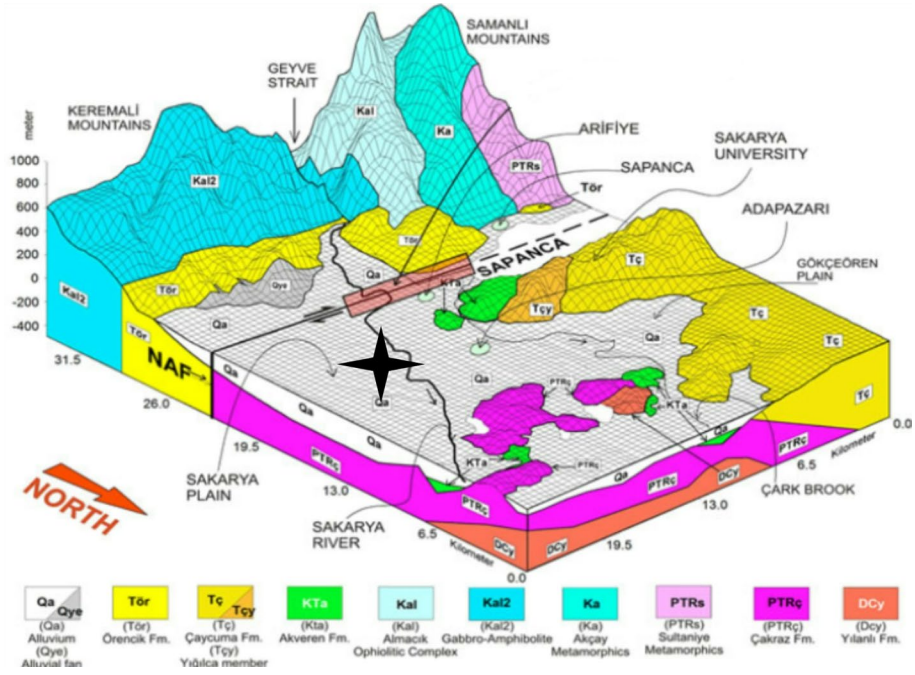


Fig. 3 3D geological map of Sakarya [37]

The foundation soil of the embankment exhibits characteristics typical of Quaternary-age sediments, predominantly composed of clay, silt, and sand. Described in the boring logs as brownish-grayish-green and moist, the soil ranges from medium stiff to stiff, occasionally containing low to high plasticity soils with fine sandy layers, fossil shells, lignite, and carbonate concretions (Fig. 5).

Figure 6 presents measured SPT-N blow counts and CPT tip resistances, while Fig. 7 shows the interpretation of soil type from CPT results, based on the study by Robertson and Campanella [22], where soil layers exhibiting predominantly sand-like behaviour are categorized as soil behaviour type 6 or higher.

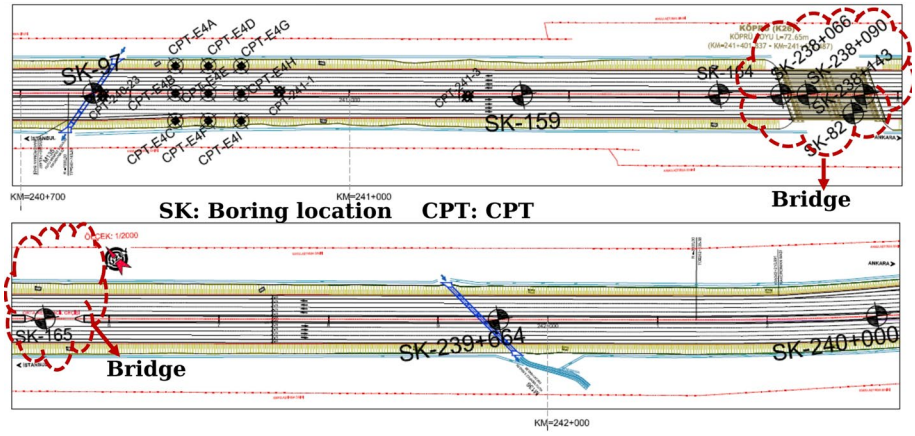


Fig. 4 Plan of in-situ test locations

Table 1 List of available tests

No	Ground investigation point	Type	Data
1	SK-82, SK-159, SK-164, SK-238 + 066, SK-238 + 090, SK-238 + 143	Exploratory borings	SPT blow counts, Laboratory tests
2	CPT-4 A, CPT-4B, CPT-4 C, CPT-4D, CPT-4E, CPT-4 F, CPT-4G, CPT-4 H, CPT-I	Cone penetration test	Dissipation tests Tip resistance and sleeve friction

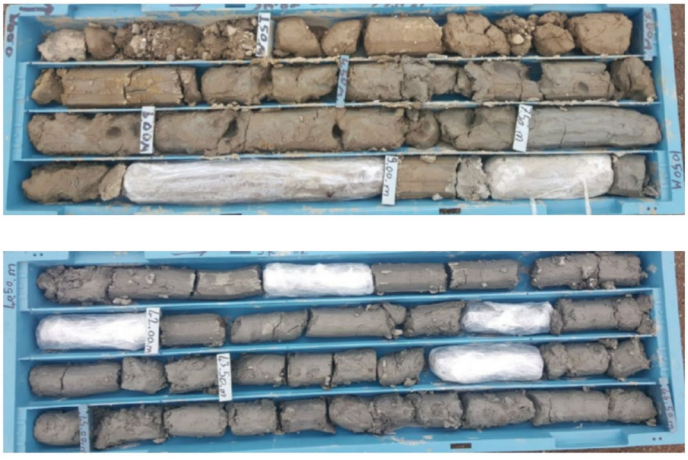


Fig. 5 View of a core box from SK-82

In addition to in-situ tests, a number of laboratory tests were conducted, including the determination of Atterberg limits and oedometer testing. The variations of plasticity indices and liquid limits with depth, as derived from soil samples, are illustrated in Fig. 8. The liquid limit values exhibit a bimodal distribution in the dataset (around ~ 40% and ~ 60%) (Fig. 9). The depth-dependent trends for compression and recompression indices are presented in Fig. 10.

The c_v values obtained from laboratory consolidation tests at different pressures are shown in Fig. 11, with maximum and minimum values of 0.00035 cm^2/s and 0.00005 cm^2/s, respectively.

The results of CPT dissipation tests that show the change in the excess water pressure due to cone penetration as a function of the square root of time are illustrated in Fig. 12.

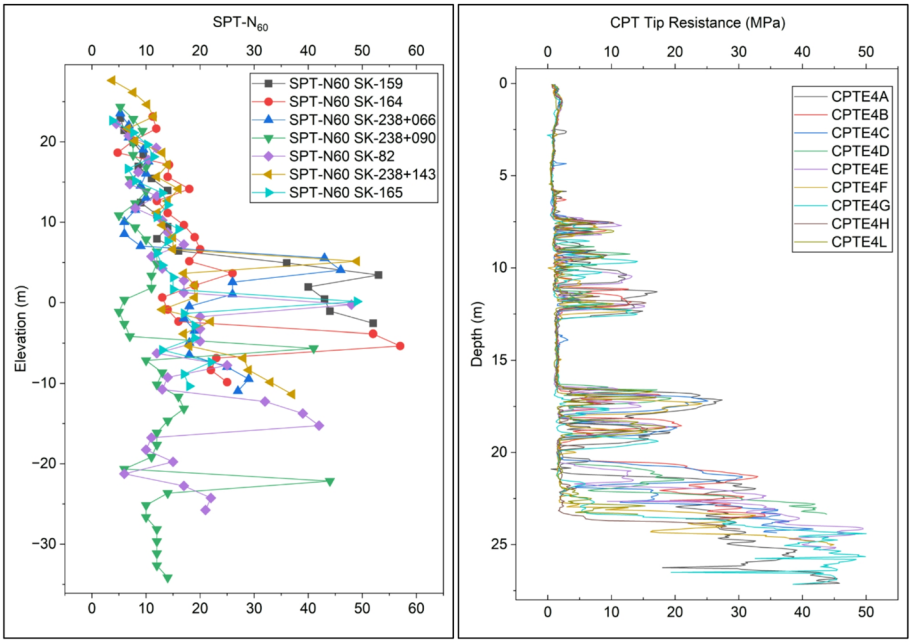


Fig. 6 In situ ground test results

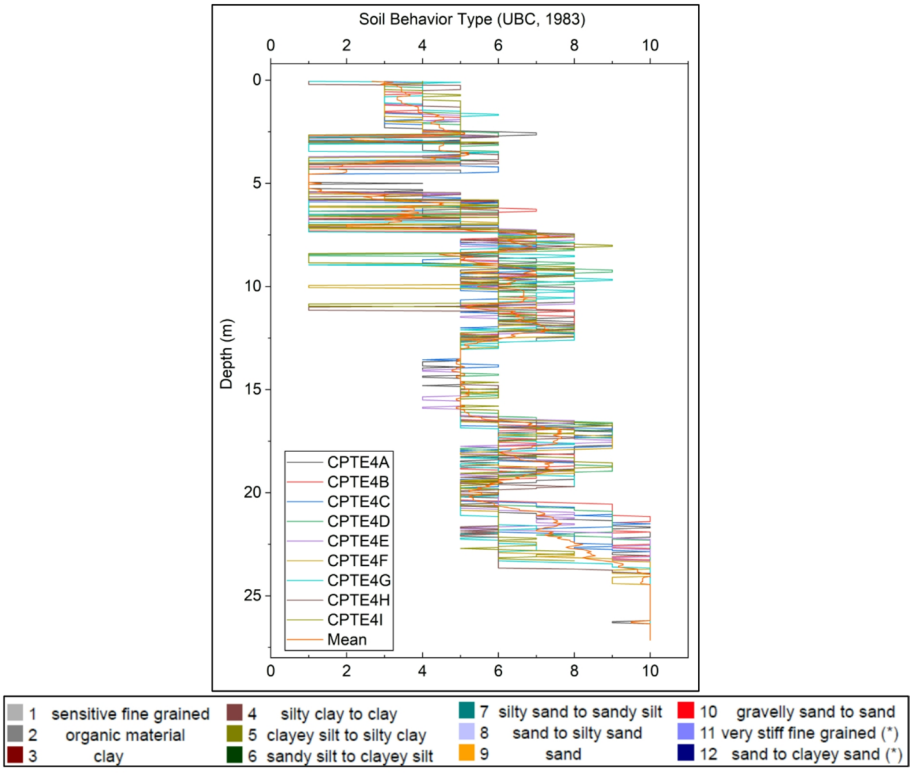


Fig. 7 Soil types according to CPT

Settlement monitoring and observed consolidation response

Field monitoring provides a necessary basis for checking settlement predictions that rely on simplifying assumptions and idealized consolidation models. Within the framework of the Observational Method (OM), originally introduced by [35] and further formalized

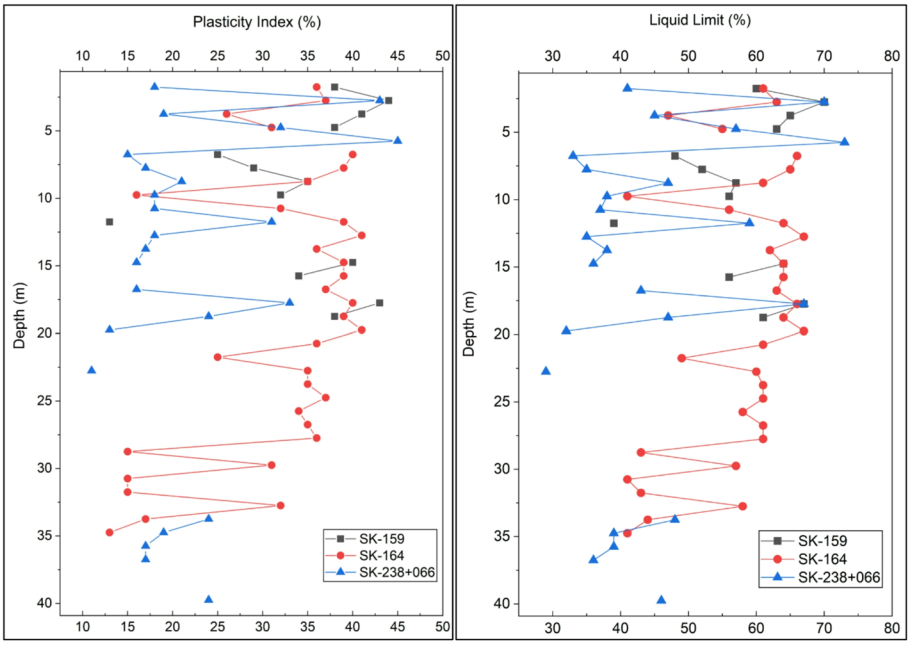


Fig. 8 Atterberg limits

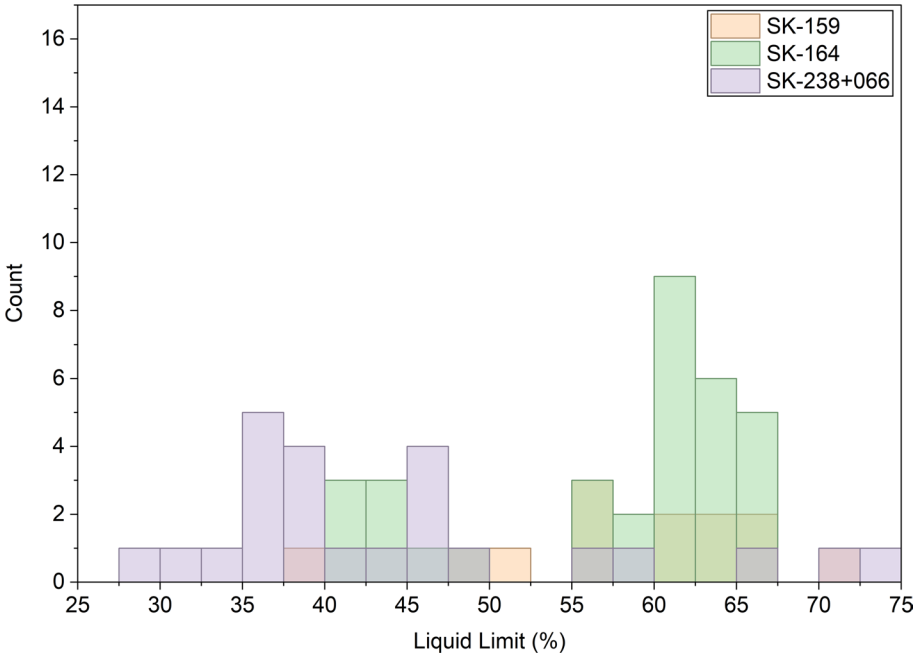


Fig. 9 Distribution of LL of embankment soil

by Peck [20], significant deviations between predicted and observed performance should motivate a reassessment of the working hypothesis and, where appropriate, an update of the design to maintain safety while improving economy [20].

To support this observational evaluation and to capture spatial variability in settlement response, thirty measurement points were installed over the embankment area, as shown in Fig. 13. During construction, some points were reported to have been lost or damaged by the contractor responsible for the monitoring programme. Moreover,

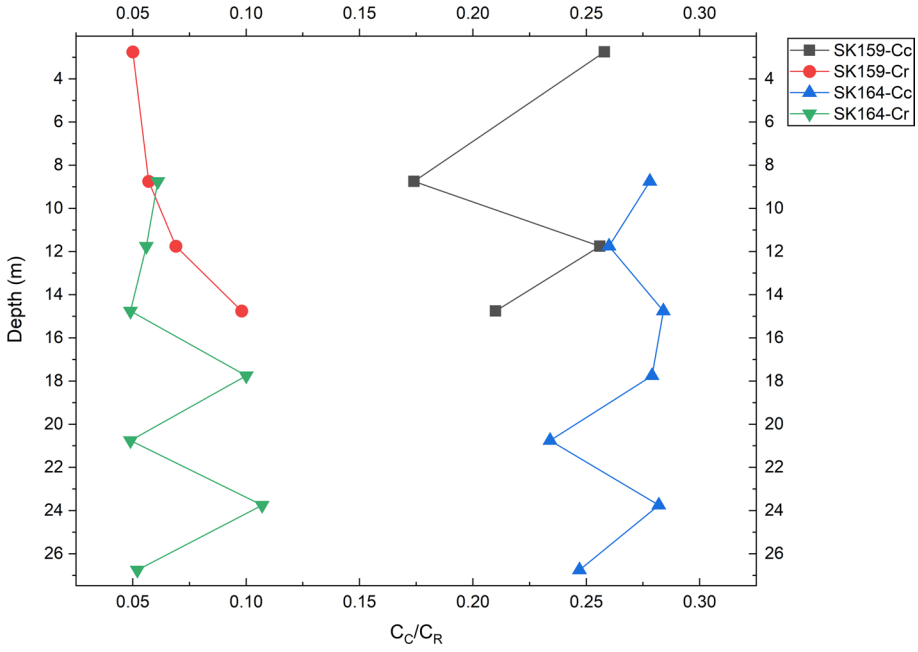


Fig. 10 Compression index, C_C and Recompression index, C_r

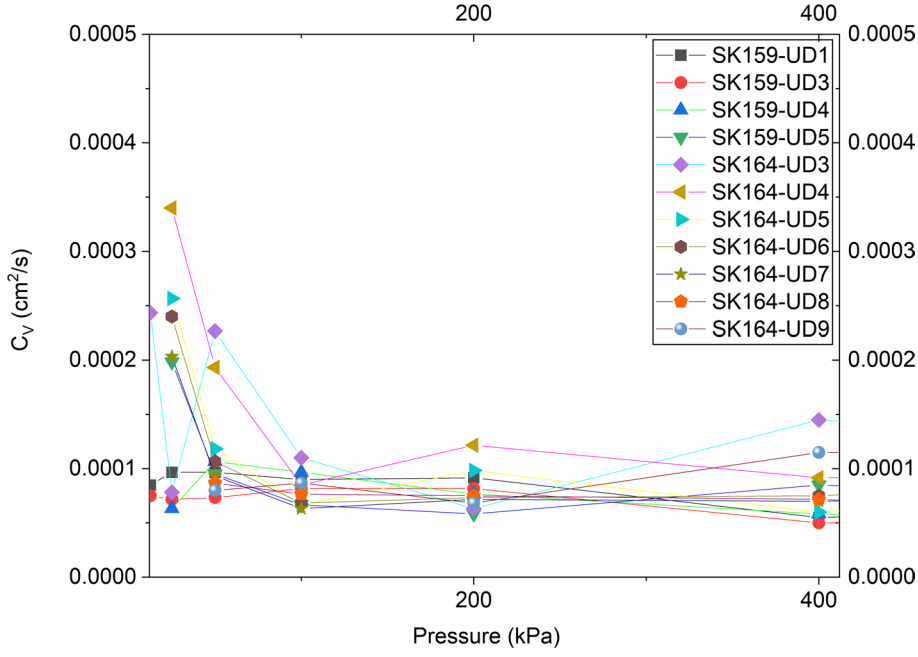


Fig. 11 c_v values from consolidation tests

for clarity, not all individual records are presented because several consolidation settlement–time curves overlap; therefore, the curves shown in Fig. 14 were carefully selected to represent the overall measurement trends, ensuring readability without sacrificing the accuracy of the data representation.

Furthermore, it should be noted that settlement readings commenced only after completion of the embankment, since the monitoring points could not be installed before

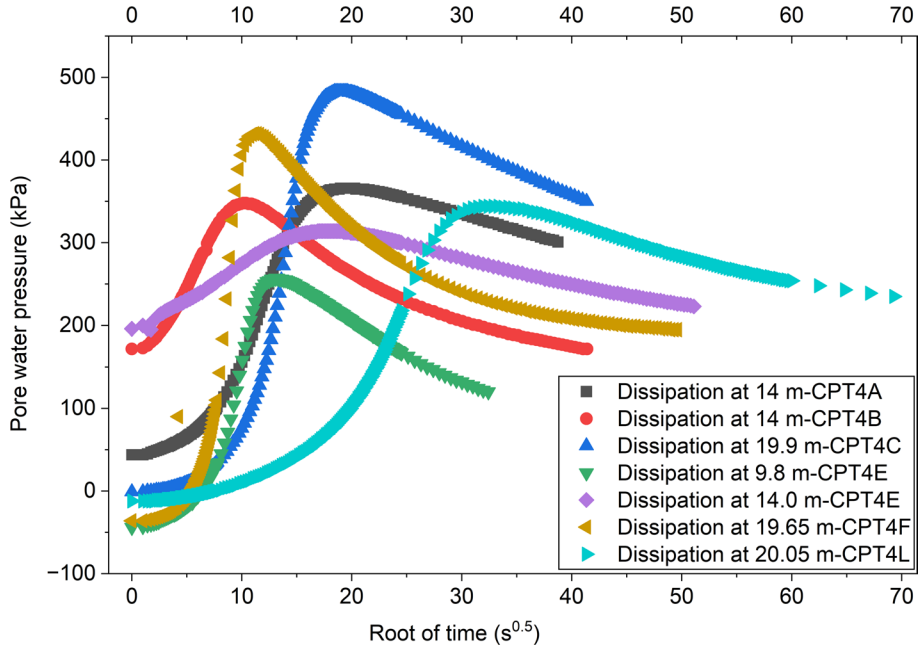


Fig. 12 CPT dissipation tests

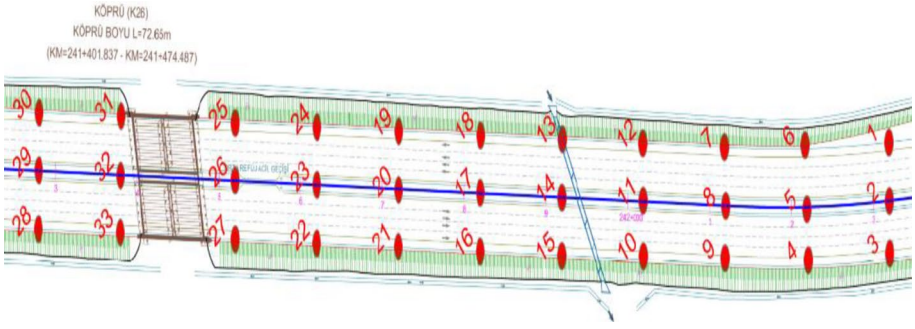


Fig. 13 Plan view of embankment with reading points

construction. Accordingly, the monitoring dataset represents the post-construction consolidation settlement increment attributable to primary consolidation (Eq. 1):

$$\Delta S\,(t) = S\,(t) - S_c \tag{1}$$

where $S\,(t)$ is the measured settlement at time t and S_c denotes the consolidation settlement occurred during the construction period prior to the first reading (i.e., the construction-stage consolidation component considered in the 1D framework). Hence, the comparisons in this study focus on consolidation behaviour inferred from the post-construction records and the corresponding back-analyses. Within this dataset, $\Delta S\,(t)$ varies along the alignment due to spatial variability in ground conditions and to changes in embankment height along the longitudinal profile.

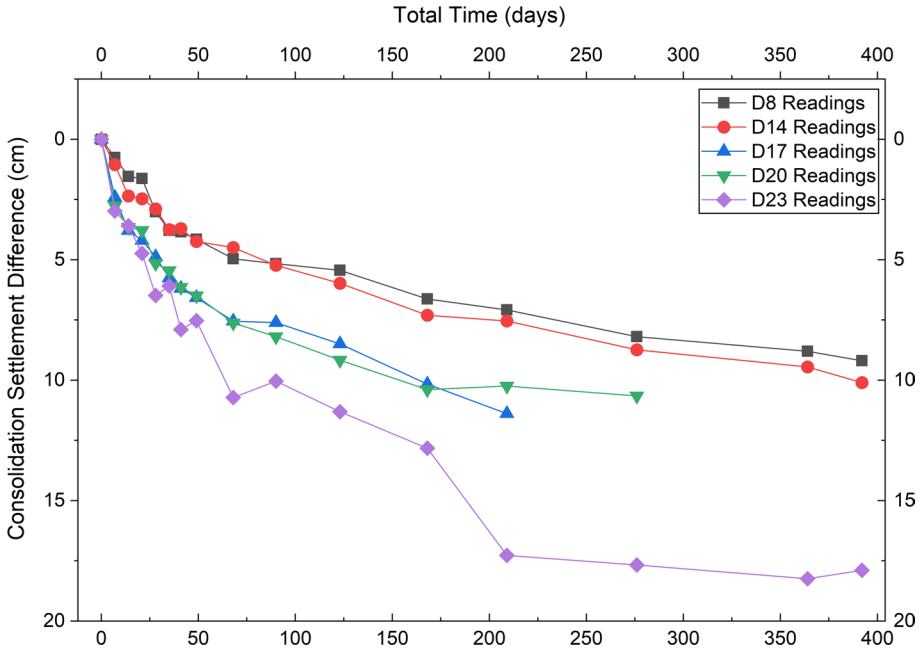


Fig. 14 Consolidation settlement readings on the embankment top surface

Methodology

This section describes the workflow used to estimate primary consolidation settlement magnitude and time rate by integrating laboratory testing, in-situ investigation (CPT/SPT and CPT dissipation), one-dimensional consolidation calculations, and observational back-analysis of consolidation settlement–time records. The methodology proceeds through (i) stress-history characterization (preconsolidation pressure and OCR), (ii) settlement magnitude calculation, (iii) determination of consolidation-rate index (c_v) from laboratory and CPT dissipation data, (iv) definition of a representative effective drainage distance (d) based on CPT-inferred stratigraphy, and application of three observational methods to monitored consolidation settlement–time curves under consistent assumptions.

Preconsolidation pressure and stress history (σ'_p, OCR): laboratory and in-situ estimation

Preconsolidation pressure (σ'_p) is a critical input for consolidation settlement assessment because soil compressibility changes markedly across the preconsolidation threshold. In this study, σ'_p is estimated from laboratory consolidation curves using two interpretation methods, and then benchmarked against empirical correlations derived from in-situ tests. This combined approach is adopted to reduce uncertainty associated with sampling disturbance and to limit operator-dependent variability inherent in graphical interpretations.

As a baseline laboratory approach, the Casagrande [7] graphical procedure is applied to the e–logσ' consolidation curve. The method identifies the point of maximum curvature and uses the standard tangent and angle-bisector construction; the intersection of the bisector with the extension of the virgin compression line provides the estimate of σ'_p. In parallel, a strain-energy-based procedure following Şenol and Sağlamer (2000), which updates the strain-energy method originally proposed by Tavenas et al., [29], is employed. In this approach, σ'_p is obtained from the intersection of the initial and final

linear segments on the $\sigma'(\Delta H/H)$–logσ' plot, where $\Delta H/H$ denotes the vertical strain. To reduce subjectivity, the linear segments are determined by regression and their intersection is computed numerically (e.g., via spreadsheet).

To provide in-situ reference values for σ'_p that are independent of laboratory sample quality (and the resulting OCR), CPT- and SPT-based empirical correlations are also adopted. Specifically, the widely applied relationships proposed by Mayne et al., [18], based on CPT tip resistance (Eq. 2), and by Mayne [17], based on SPT blow counts (Eq. 3), are implemented as follows:

$$\sigma'_p = \frac{(q_t ? \sigma_v)}{3} \tag{2}$$

$$\sigma'_p = 0.47\ (N_{60})\ \sigma_{atm} \tag{3}$$

where q_t, σ_v, N_{60}, and σ_{atm} denote the cone tip resistance, total vertical stress, SPT blow count corrected to a 60% energy ratio, and atmospheric pressure, respectively.

1D Consolidation Settlement Modelling

The consolidation settlement is computed using one-dimensional consolidation theory, with stress-history inputs taken from the OCR profiles. The analysis follows the classical 1D consolidation formulation [34] and its common engineering use for embankment settlement assessment [35, 36]. OCR–depth trends are calculated by fitted functions and used in the layer-wise settlement calculations under the embankment loading considered herein. To capture stratigraphic controls and the role of drainage boundaries, a second calculation case is evaluated in which drainage-competent sandy/silty layers are treated as drainage bands and excluded from the compressible clay thickness. These layers are identified based on CPT-derived soil behavior type (SBT) classification. This allows a direct comparison between an idealized "clay-only" profile and a stratified profile under the same loading conditions.

Estimation of coefficient of consolidation (c_v)

The coefficient of consolidation (c_v) governs the time rate of primary consolidation settlement in the classical one-dimensional consolidation framework and is often treated as a representative constant in practice [34]. Laboratory c_v is commonly obtained from incremental loading oedometer tests using the classical curve-fitting procedures of Casagrande and Fadum [8] and Taylor [31]. However, laboratory-derived rates frequently show limited agreement with field consolidation behaviour because c_v is sensitive to sampling disturbance and testing details, while field response is influenced by stratification and drainage conditions [16, 25]. Reported laboratory-to-field ratios can vary widely, from several-fold differences up to roughly two orders of magnitude. Hence, laboratory c_v values are tested against field monitoring and independent in-situ estimates to identify a representative time-rate parameter for the site. In this comparison, c_v is evaluated from (i) oedometer test interpretations, (ii) CPT dissipation tests, and (iii) LL-based correlation, and the resulting ranges are subsequently confronted with the monitored settlement–time response.

Firstly, laboratory c_v values were taken directly from the oedometer test report forms provided by the project laboratory. In these forms, c_v is evaluated using the time to 90%

consolidation (t_{90}), i.e., the Taylor $\sqrt{t}$ method. The tabulated c_v values were used as reported (with unit conversion where required), without re-interpreting the raw settlement–time curves.

Secondly, CPT dissipation tests are adopted as a practical in-situ estimate for c_v [5, 23, 32]. The tests were interpreted using the Burns and Mayne [5] SCE–CSSM solution (Eq. 4) following the procedure of Rix et al., [21]. The dissipation time was evaluated at $U = 50\%(t_{50})$ with $T'_{50} = 0.030$.

$$c_v = \frac{T\prime {a_c}^2 {I_R}^{0.75}}{t\prime} \tag{4}$$

where *T'*= Dimensionless time factor depending on degree of consolidation (*U*), a_c = radius of the probe, I_R= G/S_u= soil rigidity index, and *t'*= measured time to reach the selected *U*.

Finally, c_v was estimated from liquid limit (LL) using the power-law relationships developed by Carter and Bentley [6] based on the NAVFAC [19] LL–c_v chart. The correlations for undisturbed specimens in the recompression and virgin compression ranges are given in Eqs. 5 and 6, respectively.

$$c_v = \frac{25{,}000}{LL^{3.9}} \tag{5}$$

$$c_v = \frac{80}{LL^{2.8}} \tag{6}$$

Drainage path and equivalent drainage distance (d)

To predict the duration of consolidation settlement using Terzaghi's [34] one-dimensional consolidation theory, the selection of a representative drainage distance (d) is essential. In this study, CPT-derived soil behaviour types were used to identify layers that may act as drainage boundaries, following Robertson et al., (1983) (Fig. 7). Soil behaviour types higher than 6, broadly corresponding to sands and sand mixtures, were treated as drainage-competent layers and therefore considered potential drainage boundaries for the underlying clay strata.

Observational back-analysis of settlement–time records

Several observational methods are available to evaluate consolidation settlement–time (*S*–*t*) relationships, including the methods proposed by Asaoka [3], hyperbolic methods [26, 27, 28, 9, 10], modified Asaoka [12] and the more recent best fit method [11]. These methods involve back-analysis of consolidation settlement-time curves using various procedures. In this study, the popular methods of Asaoka [3], Modified Asaoka [12], and the recently proposed best fit method by Chung et al., [11] will be employed, and their predictive capabilities will be compared.

The method proposed by Asaoka [3] involves fitting a regression line, characterized by its intercept (β_0) and slope (β_1), along the settlement data (S_0, S_1, …, S_n) collected at a given time interval (Δt) in the S_i–S_{i+1} diagram for i = 1, 2, …, n. The ultimate settlement (S_{ult}) and the coefficient of consolidation (c_v) can then be determined using Eq. 7 and Eq. 8:

$$S_{ult} = \frac{\beta_0}{1-\beta_1} \tag{7}$$

$$c_v = \frac{-5H_D^2}{12\Delta t} ln\beta_1 \tag{8}$$

Later, Guo and Chu [12] recommended a regression line in the form of $S_i^{1.667} = \beta_0 + \beta_1 S_{i+1}^{1.667}$ such that (Eqs. 9 and 10):

$$S_{ult} = \left(\frac{\beta_0}{1-\beta_1}\right)^{0.6} \tag{9}$$

$$c_v = \frac{-H_D^2}{2\Delta} ln\beta_1 \tag{10}$$

The method by Chung et al., [11] utilizes Taylor's model as a substitute for Terzaghi's solution to best-fit through either the full or a partial range of the time–settlement data, and includes two distinct equations (Eq. 11 and Eq. 12):

$$S = S_{100}\left[\sqrt{\frac{4xt}{\pi}} + (1 - 10^{\left\{\frac{-(xt+0.851)}{0.933}\right\}}\right] \tag{11}$$

$$y_{1D} = -\log\left(1 - \frac{S - S_0}{S_{ult} - S_0}\right) = \frac{\mathrm{x\,(t - t_0)}}{0.933} + 0.0912 \tag{12}$$

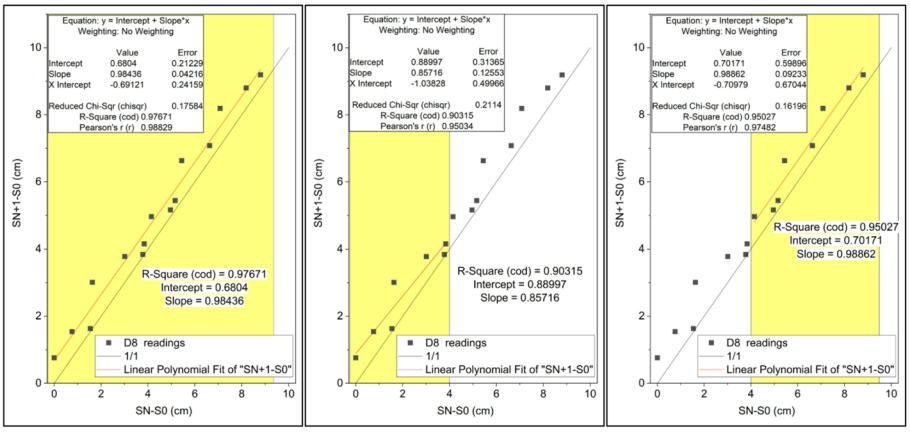
where S is the settlement at time t; S_0 and t_0 denote the settlement and time at the start of the fitted record (so that t is taken as elapsed time from t_0); H_D is the representative drainage distance consistent with the adopted drainage model; $T_v = c_v \mathrm{t}/\mathrm{H_D^2}$ is the dimensionless time factor and $x = c_v/H_D^2$ (hence $T_v = x\,t$); $t_{60} = T_{v,60}/x = 0.287/x$. Here, S_{100} denotes the settlement at $U = 100\%$ in Taylor's formulation and corresponds to the ultimate consolidation settlement (primary component); hence, $S_{100} \equiv S_{ult}$ in Eqs. 11 and 12.

Results and discussion

Observational back-analysis: method comparison and window sensitivity

Regression lines based on Asaoka's method (1978) are presented for the D8 settlement–time record (ΔS–t) using three sampling windows—0–49 days, 49–392 days, and 0–392 days—as illustrated in Fig. 15a, b,c. The results demonstrate that the adopted sampling range exerts a pronounced influence on the fitted regression line and, consequently, on the inferred (S_{ult}?S_c), yielding substantially different regression coefficients β_0 and β_1 when the early-stage, late-stage, or full-duration data are considered. The resulting (S_{ult}?S_c) and the corresponding c_v estimates derived from each sampling window are summarized in Table 2. For consistency, the sampling-window sensitivity plots were limited to Asaoka's method; the corresponding plots for Guo and Chu [12] are omitted for brevity. All observational back-analyses in this section adopt a representative drainage distance of $d = 3.75$ m.

The Asaoka method yields broad ranges of (S_{ult}?S_c) for D8 (6.23–61.55 cm), D14 (4.73–285.17 cm), and D17 (2.83–17.15 cm), and in several cases produces negative



(a) (b) (c)

Fig. 15 Application of Asaoka [3] method to D8 for sampling range of **a** 0-392 days, **b** 0–49 days and **c** 49–392 days

Table 2 Estimated S_{ult}-S_c and c_v values from Asaoka, Guo and Chu [12] and Chung et al., [11] methods for d = 3.75 m

Reading Points	Duration (days)	$(S_{ult}\text{-}S_c)_{est}$ (cm)			c_v (cm^2/s)		
		Asaoka	Guo and Chu	Chung	Asaoka	Guo and Chu	Chung
D8	0-392	43.62	N.A.*	9.06	0.0004	N.A.*	0.0039
	0–49	6.23	N.A.*	3.86	0.0149	0.0032	0.0042
	49–392	61.55	11.76	8.90	0.0002	N.A.*	0.0043
D14	0-392	285.17**	N.A.*	10.01	0.0001	N.A.*	0.0024
	0–49	4.73	7.13	4.07	0.0280	0.0089	0.0026
	49–392	N.A.*	N.A.*	9.98	N.A.*	N.A.*	0.0024
D17	0-209	17.15	N.A.*	11.16	0.0033	N.A.*	0.0064
	0–49	6.83	3.46	6.65	0.0373	0.0124	0.0045
	49–209	2.83	9.64	11.08	N.A.*	N.A.*	0.0061
D20	0-276	11.55	66.66	10.70	0.0051	0.0001	0.0101
	0–49	6.37	8.55	6.55	0.0445	0.0161	0.0105
	49–276	11.59	11.97	10.77	0.0048	0.0045	0.0118
D23	0-392	26.55	885.61**	18.59	0.0018	0.0000	0.0042
	0–49	12.34	20.20	7.78	0.0193	0.0271	0.0028
	49–392	19.74	8.37	18.19	0.0035	0.0033	0.0052

* Calculated negative values are designated as N.A. (Not Applicable)

** The back-calculated settlement predictions, which are approximately four times higher than the observed settlements, are deemed to have diverged from the measured response and are therefore excluded from the subsequent figures

$(S_{ult}?S_c)$ and/or c_v, indicating non-convergent fits for those records. In contrast, the estimates for D20 (6.37–11.59 cm) and D23 (12.34–26.55 cm) are comparatively stable. This sensitivity is also apparent for D8, where the measured post-construction settlement is about 9 cm: the upper-end Asaoka estimates imply an overprediction on the order of five to seven times, depending on the sampling window.

The same settlement–time records were also analysed with the modified Asaoka formulation proposed by Guo and Chu [12] (Table 2). For this dataset, the method exhibits more frequent convergence issues than original Asaoka: for both D8 and D14, two out of three sampling windows yield negative $(S_{ult}?S_c)$and/or $c_v$values and are therefore reported as N.A. In addition, the method can produce unrealistically large estimates for

certain windows; for example, the D23 (0–392) case yields $(S_{ult} - S_c) = 885.61$ cm and is flagged as diverged, and is therefore excluded from subsequent figures following the criterion stated below the table. Overall, relative to the original Asaoka method, the Guo and Chu [12] formulation yields a higher rate of non-applicable and diverged fits in this dataset, limiting its consistency across records.

Similarly, the best-fit algorithm of Chung et al., [11] was applied to the same data sets for comparison with two observational methods (Table 2). The fitted curves for D8, D14, D17, D20, and D23 across the investigated sampling windows are also shown in Fig. 16. Overall, the method yields $(S_{\mathrm{ult}}?S_c)$ estimates of 3.86–18.59 cm and corresponding c_v values of 0.0024–0.0118 cm²/s. In contrast to the Asaoka [3, 12, 11] method does not produce negative $(S_{\mathrm{ult}}?S_c)$or c_v values (hence no N.A. entries) and are not flagged as diverged under the adopted criterion, while remaining comparatively stable with respect to the sampling window. Although the estimated parameters exhibit some sensitivity to the selected sampling window, the results are internally more consistent than those obtained from the Asaoka [3] and Guo and Chu [12], as reflected by the comparatively bounded c_v ranges and the absence of non-physical outcomes. Nevertheless, practical screening and fitting strategies can be adopted to further reduce the remaining sampling-window dependence and to improve the robustness of $(S_{ult}?S_c)$and c_v identification.

Although the Chung-based fits are comparatively stable across sampling windows, the method still involves two unknowns that must be identified jointly: the ultimate post-construction increment $(S_{ult}?S_c)$ and the coefficient of consolidation c_v. Because these parameters are calibrated simultaneously, the back-analysis is not strictly unique; different $(S_{ult} - S_c$,$\mathrm{c_v})$ pairs can reproduce the same settlement–time record with similar fit statistics (e.g., $R^2$and SSE), as summarized in Table 3. This trade-off is evident when S_{ult}

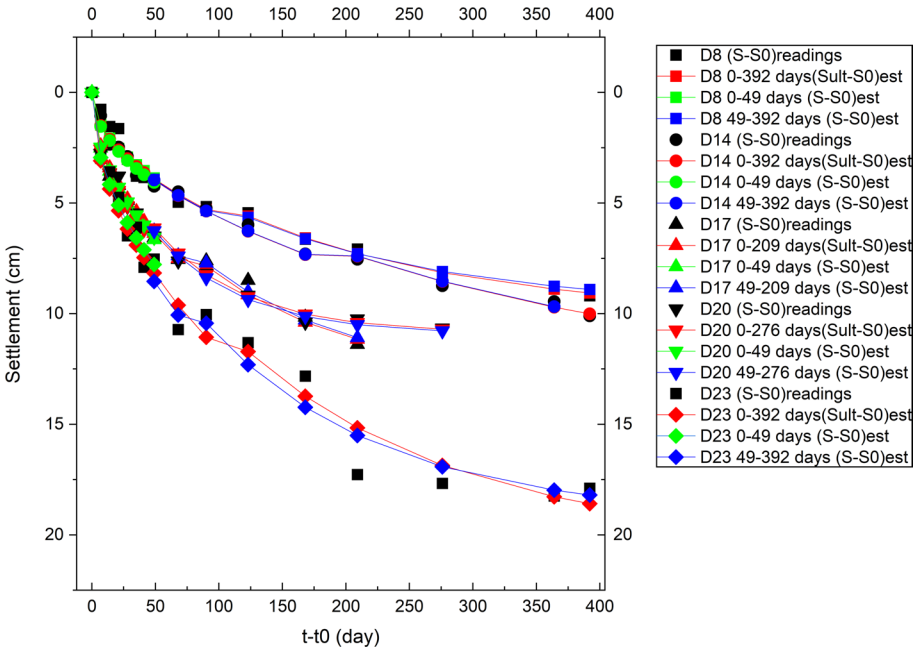
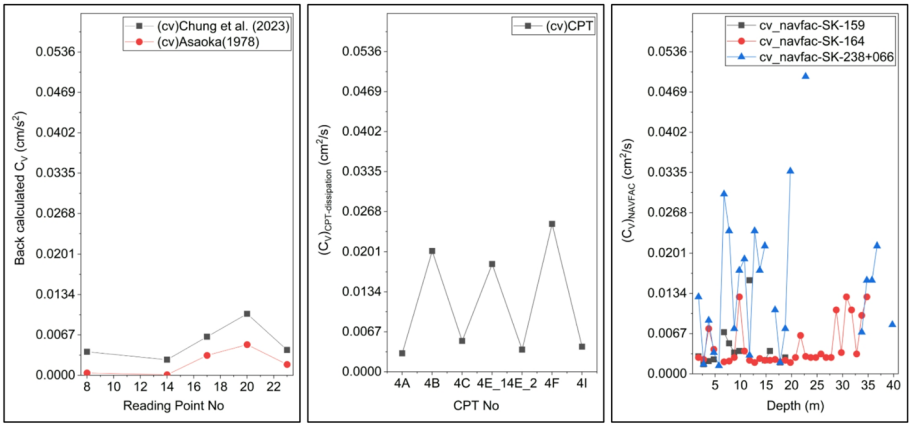


Fig. 16 Application of Chung et al., [11] method to D8, D14, D17, D20 and D23 readings

Table 3 R^2 and sum of the squared errors (SSE) of regression curves

D23-No iteration of S_{ult} and iteration of c_v					D23-Iteration of both and S_{ult} and c_v			
Duration	0-392 days	0–49 days	49–392 days	d (cm)	Duration	0-392 days	0–49 days	49–392 days
$(c_v)_{est}$=	0.0014	0.0015	0.0016	350	$(c_v)_{est}$=	0.0034	0.0036	0.0037
	0.0018	0.0020	0.0021	400		0.0044	0.0048	0.0049
$(S_{ult-}S_c)_{est}$:	30.00	30.00	30.00		$(S_{ult-}S_c)_{est}$:	20.33	23.76	19.14
R^2	97.7%	96.1%	89.1%		R^2	97.6%	96.2%	92.0%
SSE	12.333	1.731	17.307		SSE	11.159	1.720	8.423



a) b) c)

Fig. 17 Comparison of c_v predictions from **a** observational methods, **b** CPT dissipation tests and **c** NAVFAC LL-based (recompression line/OC state)

is constrained: prescribing a fixed S_{ult} (e.g., 30 cm) across sampling windows drives the fit toward systematically smaller c_v values—sometimes less than half of those obtained when $(S_{ult}?S_c)$ and c_v are estimated together within the same optimisation. In addition, adopting an unrealistically low c_v (for example, half of a representative value) forces the fit toward a larger $(S_{ult}?S_c)$ and, in turn, an exaggerated consolidation time scale relative to field observations. For this reason, the calibration should be constrained using realistic in-situ evidence—most importantly c_v from CPT dissipation. The NC/OC classification is also required when using LL-based c_v correlations, since the appropriate relationship differs between recompression (OC) and virgin compression (NC) ranges. These constraints reduce non-uniqueness and improve settlement-duration predictions when applying the [11] best-fit approach.

Coefficient of consolidation (c_v): estimates and comparison

In Fig. 17a, the coefficient of consolidation (c_v) values derived through two observational methods (Asaoka and Chung) are compared with those obtained from CPT dissipation tests in Fig. 17b and the NAVFAC [19] LL-c_v chart (recompression/OC range) using the power-law approximations proposed by Carter and Bentley [6], plotted as depthwise profiles in Fig. 17c. Again, the c_v values from the best-fit regression assume an average drainage distance of 3.75 m, and a single representative c_v value governing the settlement behavior.

It is seen from figures that the lower values from the CPT dissipation tests are closest to the back-calculated c_v values. Additionally, the c_v estimates associated with higher LL

values (i.e., lower inferred c_v) show a closer match to the back-calculated ones. These results suggest that the layers with lower CPT dissipation test results or higher LL values exerted a greater influence on the consolidation settlement-time behavior. Therefore, when estimating the settlement duration of a layered clayey soil with varying characteristics using the traditional 1-D Terzaghi consolidation equation, it is essential to provide a cautious estimate of c_v which should be based on both CPT dissipation tests and LL-based predictions such as those from NAVFAC [19], considering that high-LL layers can significantly dominate the consolidation behavior.

In addition, it is understood that the layers or bands assumed to behave as drainage boundaries should be effectively investigated with a series of CPT and dissipation tests. These tests can reveal the continuity of the layers and their permeability characteristics. In this study, drainage boundaries and distances were assumed based on CPT soil classification numbers. Soils classified higher than number 6 were assumed to have the potential to act as drainage bands in clayey soil. Subsequent dissipation tests at random depths (without attempting to target potentially thin CPT-indicated layers) indicated that c_v can be at least five times higher in some intervals than in adjacent layers, supporting the interpretation that some intervals may reasonably act as drainage-competent bands within the clayey profile. The results are consistent with the assumption that a representative drainage distance of ~3.75 m governs the settlement–time behaviour (within the examined 3.5–4.0 m range). To further verify this conclusion, the drainage distance was also investigated by back-analyzing the settlement-time graphs using the best fit approach. The back analyses confirmed that this drainage distance is valid, as the back-calculated c_v values are consistent with the lower values of dissipation tests results and LL based prediction, as shown in Fig. 17a, b and c.

Moreover, Table 4 summarizes the estimated time required to reach 90% primary consolidation (U = 90%) by combining alternative c_v sources (CPT dissipation, laboratory consolidation tests, and NAVFAC [19] LL–c_v recommendations) with the observed consolidation settlement durations. For the CPT-derived c_v range, the predicted consolidation time spans from 57 to 393 days depending on the adopted drainage distance and the representative c_v value. However, the CPT lower-average c_v (around 0.0040 cm^2/s) yields durations of 301–393 days (d = 3.5–4.0 m), which are broadly consistent with the observed time window (170–400 days), whereas the CPT higher-average c_v (around 0.021 cm^2/s) results in markedly shorter durations (57–75 days). Laboratory-based c_v values (0.00035 cm^2/s) predict substantially longer consolidation times (3435–4487 days;

Table 4 c_v and consolidation time for different scenarios

c_v (cm^2/s)	Drainage Dist. (m)	Duration for U = 90% (days)
CPT Lower average:0.0040	3.5	301
CPT Higher average:0.021		57
CPT Lower average:0.0040	4.0	393
CPT Higher average:0.021		75
Lab oedometer maximum: 0.00035	3.5	3435 (9.4 years)
Lab oedometer maximum: 0.00035	4.0	4487 (12.3 years)
NAVFAC, [19] on recompression line for *LL* = 60: 0.0035	3.5	344
NAVFAC, [19] on recompression line for *LL* = 40: 0.015		80
NAVFAC, [19] on recompression line for *LL* = 60: 0.0035	4.0	449
NAVFAC, [19] on recompression line for *LL* = 40: 0.015		105
Consolidation settlement reading intervals		Minimum ≈ 170
		Maximum ≈ 400

9.4–12.3 years), corresponding to approximately 9–12 times the observed upper-bound duration and indicating poor compatibility for settlement-duration prediction in this case. Finally, NAVFAC [19] recompression-line guidance brackets the time scale: the LL = 60 recommendation (c_v = 0.0035 cm²/s) gives durations of 344–449 days, consistent with the CPT lower-average estimate and the observations, whereas LL = 40 recommendation (c_v = 0.015 cm²/s) yields shorter durations (80–105 days) than observed. This suggests that the higher-LL band (LL ≈ 60) is more representative of the field-governing time scale.

Settlement magnitude: predictions vs. observations

Figure 18 compares post-construction primary consolidation settlement increments, $(S_{ult}?S_c)$, back-analysed from the same settlement records using three observational procedures [3, 11, 12]. The figure highlights clear method-to-method differences for identical monitoring points. The Guo and Chu [12] procedure yields non-applicable (non-convergent) outputs for several records (e.g., D8 and D14; see Table 2), which prevents its use as a consistent interpretation method across the full set of points. The Asaoka [3] method produces feasible estimates more broadly, but the inferred $(S_{ult}?S_c)$ shifts with the fitting window and reading interval; truncation or resampling of the same record can therefore change the estimated ultimate settlement. In contrast, the theory-constrained best-fit procedure of Chung et al., [11] exhibits lower window sensitivity over the ranges examined here, since the interpretation is carried out by fitting the measurements to a prescribed consolidation curve rather than extrapolating from discrete readings alone.

Table 5 links the observational back-analysis to 1D consolidation calculations by using the best-fit c_v estimates to compute both the construction-stage component S_c (for the six-day construction period) and the corresponding ultimate settlement (S_{ult}). The table

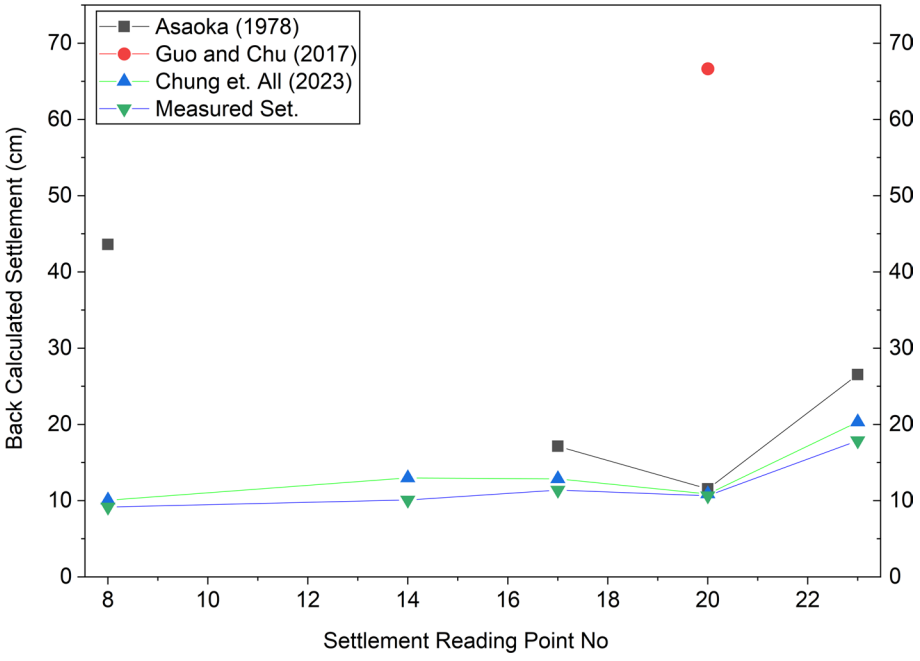


Fig. 18 Comparison of S_{ult}-S_c values with settlement readings

Table 5 Ultimate consolidation settlement (S_{ult}-S_c and $S_{ult\text{-}Chung}$) based on back analyzed c_v values

Reading points	$(c_v)_{fit}$ cm^2/s	S_{ult}-S_c (cm)	T_V	U_V %	$S_{ult-Chung}$ (cm)	H_{fill} (m)	$(S_{con})_{Şenolmin}$ (cm)	Ratio
D8	0.004	10.08	0.0072	0.096	11.15	4.0	13.3	1.19
D14	0.003	12.99	0.0046	0.077	14.07	4.5	14.8	1.05
D17	0.007	12.87	0.0120	0.124	14.68	5.0	16.2	1.10
D20	0.010	10.89	0.0188	0.155	12.88	5.0	16.2	1.26
D23	0.004	20.33	0.0079	0.100	22.60	5.5	17.6	0.78

also reports theoretical settlement magnitudes obtained from OCR profiles inferred with the Şenol method, together with a stratigraphically informed variant in which CPT-classified drainage-competent sandy/silty layers are excluded from the compressible clay thickness ($S_{con})_{Şenolmin}$). This stratigraphic refinement brings the Şenol-based theoretical settlements into closer agreement with the Chung-based ultimate consolidation settlements $(S_{ult,\mathrm{Chung}})$, indicating that how the compressible profile is idealized (and, implicitly, how drainage-competent layers are treated) has a first-order impact on predicted ultimate settlement. As summarized in Table 5, the ratio $(Sc)_{Şenol,\ min}$ / $S_{ult,\ Chung}$ ranges from approximately 0.78 to 1.26 across the considered measurement points, corresponding to deviations on the order of about – 22% to + 26%.

Figure 19 offers an independent comparison between corrected settlements derived using the Chung-based c_v and theoretical settlements computed from OCR profiles interpreted using the Şenol and Casagrande procedures. The Casagrande-based OCR leads to substantially larger settlements—on the order of three to four times the corrected ultimate primary consolidation values—highlighting the sensitivity of the Casagrande construction to curve shape and operator judgment when the e–$\log\sigma'$ relationship is affected by sampling disturbance and the point of maximum curvature is not clearly defined. By contrast, consolidation settlements computed with the Şenol-derived OCR fall close to the corrected ultimate values. This agreement improves further under the "clay-only" idealization, where CPT-classified drainage-competent sandy/silty layers are excluded from the compressible thickness.

Taken together, Figs. 18 and 19, and Table 5 show that prediction reliability in layered soft deposits is governed less by the formal calculation scheme than by how stress history and stratigraphy are translated into model inputs. Figure 18 indicates that observational back-analysis can be window-dependent and, for some records, method-limited; when monitoring is short or irregular, a theory-constrained best-fit procedure [11] provides the most consistent interpretation of $(S_{ult}?S_c)$. Figure 19; Table 5 show that settlement magnitude is controlled primarily by the adopted OCR interpretation and by whether CPT-classified drainage-competent sandy/silty layers are included in the compressible thickness. Excluding these layers ("clay-only" idealization) brings theory-based settlements close to the corrected ultimate values. Therefore, a more reliable basis for design is obtained by applying the integrated framework adopted in this study: stress-history (OCR) interpretation, a stratigraphy-informed representation of the compressible profile and drainage path, and observational back-analysis.

5. Conclusions

This paper presents a case-history comparison of laboratory-, in-situ-, and monitoring-based methods for predicting the magnitude and duration of primary consolidation settlement for the NMH/KMO embankment. Because settlement monitoring commenced

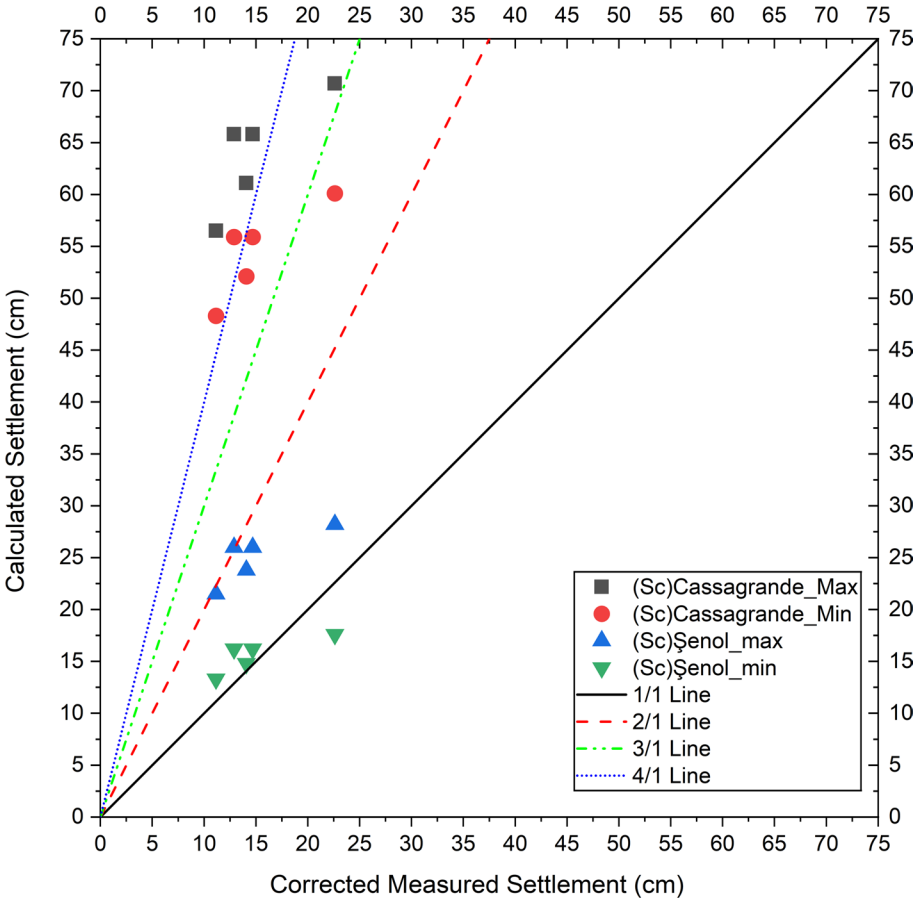


Fig. 19 Comparison of corrected settlements ($S_{ult\text{-}Chung}$) with calculated values by using Şenol and Casagrande methods

only after completion of the embankment, the comparisons are primarily framed in terms of the post-construction consolidation settlement increment, $(S_{ult}?S_c)$. The main conclusions are as follows:

- In this case history, OCR interpretation drives substantial variability in predicted settlements; the regression-supported, energy-based procedure (Şenol method) provides a more consistent basis for OCR profiling, and agreement with the monitored response improves when drainage-competent sandy/silty layers are excluded from the compressible clay thickness.
- Translating CPT-derived stratigraphy into a drainage model (i.e., identifying drainage-competent bands and their continuity) is a key modelling choice, and it can shift predicted consolidation durations markedly even for comparable c_v ranges. Drainage boundaries and representative drainage distances inferred from CPT-based soil classification provide a practical basis for defining the controlling drainage path in stratified deposits.
- For the representative drainage-distance range inferred for this site (about $d = 3.5$ –4.0 m), the lower-average CPT-dissipation estimate (c_v≈0.0040 cm^2/s) yields $U = 90\%$ durations of about 301–393 days, broadly consistent with the observed settlement-duration window (≈ 170–400 days). In contrast, the laboratory-derived value used in the paper (c_v≈0.00035 cm^2/s) predicts multi-year durations (≈ 9.4–12.3

years), indicating poor representativeness for field-scale time-rate prediction in this deposit. For NAVFAC LL–c_v guidance on the recompression line, the outcome depends on the selected LL trend: the higher-LL trend (LL≈60%, c_v ≈0.0035 cm^2/s) yields durations (≈ 344–449 days) consistent with the dissipation-based estimate and the observed time scale, whereas the lower-LL trend (LL≈40%, c_v ≈0.015 cm^2/s) predicts substantially shorter durations than observed.

- In this dataset, the classical Asaoka [3] and Guo and Chu [12] procedures were sensitive to the selected time window and produced non-physical/non-convergent outputs for some records, whereas the theory-constrained best-fit approach [11] provided comparatively consistent estimates across the investigated sampling ranges.
- From a design perspective, design reliability improves when OCR is established first (Şenol method with in-situ checks), CPT-derived stratigraphy is translated into an explicit drainage model to define the representative drainage distance, and c_v is then constrained using dissipation-derived indices and LL-based guidance, with monitoring used for calibration where available.

Author contributions
1-Alparslan DOĞAN: Conceived and designed the analysis; Contributed data or analysis tools; Performed the analysis; Wrote the paper. Corresponding Author.2-S. Oğuzhan AKBAŞ: Supervised the analysis; Reviewed and wrote the paper.

Funding
The authors received no financial support for the research, authorship, and/or publication of this article.

Data availability
The authors confirm that all data generated or analyzed during this study are included in this published article. In addition, data shall be available on request in a variety of formats, including Excel.

Declarations

Competing interests
The authors declare no competing interests.

Received: 2 April 2025 / Accepted: 23 February 2026
Published online: 12 March 2026

References

1. Abu-Farsakh MY, Yu X, Gautreau G (2011) Control of Embankment Settlement Field Verification on PCPT Prediction Methods. *Louisiana Transportation Research Center (LTRC)*. Final Report (Report No. FHWA/LA.10/476)
2. Arroyo M, Mateos T (2006) Embankment design with DMT and CPTu: prediction and performance. *Proceedings from the Second International Flat Dilatometer Conference*. 62–68
3. Asaoka A (1978) Observational Procedure of Settlement Prediction. Japanese Society of Soil Mechanics and Foundation Engneering Soils And Foundations. 18(1):87–101
4. Beyen K, Erdik M (2004) Two-dimensional nonlinear site response analysis of Adapazarı plain and predictions inferred from aftershocks of the Kocaeli earthquake of 17 August 1999. Soil Dyn Earthq Eng 24(3):261–279
5. Burns SE, Mayne PW (2002) Analytical Cavity Expansion-Critical State Model for Piezocone Dissipation in Fine-Grained Soils. Soils Found Japanese Geotech Soc 42(2):131–137
6. Carter M, Bentley SP (2016) Soil Properties and their Correlations. Second Edition. *John Wiley & Sons, Ltd*
7. Casagrande A (1936) The Determination of the Pre-Consolidation Load and Its Practical Significance. Proc 1st Int Conf Soil Mech D–34:60–64
8. Casagrande A, Fadum RE (1940) Notes on Soil Testing for Engineering Purposes. Harv Soil Mech Ser No 8
9. Chung S-G, Lee N-K, Kim S-R (2009) Hyperbolic method for prediction of prefabricated vertical drains performance. J Geotech GeoEnviron Eng 135(10):1519–1528
10. Chung S-G, Kweon H-J, Jang W-Y (2014) Observational method for field performance of prefabricated vertical drains. Geotext Geomembr 42(4):405–416
11. Chung SG, Kweon HJ, Chung CG (2023) Back-analysis of one-dimensional consolidation settlement. Acta Geotech 19:239–254
12. Guo W, Chu J (2017) New observational method for prediction of one-dimensional consolidation settlement. Geotechnique 67(6):516–522
13. Kim SY, Lee J-S, Hong W-T (2021) Subgrade assessment using automated dynamic cone penetrometer to manage geo-infrastructures. Smart Struct Syst 27(5):861–870

14. Kim SY, Lee J-S, Park G-W, Hong W-T (2022) Evaluation of dynamic resistance for application of portable in-situ device to extra target depth. KSCE J Civ Eng 26(10):4195–4201
15. Lee J-S, Jeong SH, Park G, Kim YS, Tutumluer E, Kim SY (2025) Geotechnical application of unmanned aerial vehicle (UAV) for estimation of ground settlement after filling and compaction. Transp Geotechnics 51:101517
16. Leroueil S (1988) Tenth Canadian Geotechnical Colloquium: recent developments in consolidation of natural clays. Can Geotech J 25:85–107
17. Mayne PW (2007a) In-Situ Test Calibrations for Evaluating Soil Parameters. Charact Eng Prop Nat Soils 3:1602–1652
18. Mayne PW, Coop MR, Springman S, Huang A-B, and Zornberg J., State-of-the-Art Paper (SOA-1): Geomaterial Behavior and Testing. Proceedings of the 17th International Conference on Soil MechanicsGeotechnical Engineering, (ICSMGE, Alexandria (2009) Millpress/IOS Press Rotterdam. 4: 2777–2872
19. NAVFAC (1986) Design Manual 7.01 - Soil Mechanics. Department of the Navy, Naval Facilities Engineering Command, Alexandria, VA
20. Peck RB (1969) Advantages and limitations of the Observational Method in applied soil mechanics. Ninth Rankine Lecture Géotechnique 19:171–187
21. Rix GJ, Wainaina N, Ebrahimi A, Bachus RC, Limas M, Sancio R, Fait B, Mayne PW (2019) Manual on Subsurface Investigations. NCHRP Web-Only Doc *258*
22. Robertson PK, Campanella RG (1983). Interpretation of Cone Penetration Tests: Sands and Clays. Can Geotech J 20(4):719–745
23. Robertson PK, Sully JP, Woeller DJ, Lunne T, Powell JJM, Gillespie DG (1992) Estimating coefficient of consolidation from piezocone tests. Can Geotech J 29:539–550
24. Şenol A, Sağlamer A 2000. Determination of Preconsolidation Pressure with a New Strain Energy –Log Stress Method. Electron J Geotech Eng 5: 1–11
25. Shukla S, Sivakugan N, Das B (2009) Methods for determination of the coefficient of consolidation and field observations of time rate of settlement — an overview. Int J Geotech Eng 3(1):89–108
26. Tan T-S, Inoue T, Lee S-L (1991) Hyperbolic method for consolidation analysis. J Geotech Eng 117(11):1723–1737
27. Tan S-A (1995) Validation of hyperbolic method for settlement in clays with vertical drains. Soils Found 35(1):101–113
28. Tan S-A, Chew S-H (1996) Comparison of the hyperbolic and Asaoka observational method of monitoring consolidation with vertical drains. Soils Found 36(3):31–42
29. Tavenas F, Des Rosiers J-P, Leroueil S, Rochelle P, La, Roy M (1979) The use of strain energy as a yield and creep criterion for lightly overconsolidated clays. Géotechnique 29(3):285–303
30. Tavenas F, Leblond P, Jean P, Leroueil S (1983) The permeability of natural soft clays. Part I: methods of laboratory measurement. Can Geotech J 20(4):629–644
31. Taylor DW (1948) Fundamentals Of Soil Mechanics. Wiley
32. Teh CI, Houlsby GT (1991) An analytical study of the cone penetration test in clay. Géotechnique 41(1):17–34
33. Robertson PK, Sully JP, Woeller DJ, Lunne T, Powell JJM, Gillespie DG (1992) Estimating coefficient of consolidation from piezocone tests. Can Geotech J 29(4):539–550
34. Terzaghi K, Erdbaumechanik (1923) *Franz Deuticke, Vienna*
35. Terzaghi K, Peck RB, Mesri G (1996) Soil Mechanics in Engineering Practice, 3rd edn. Wiley, New York
36. USACE (1990) Settlement Analysis. Engineer Manual (EM) 1110-1-1904. *Department of the Army, U.S. Army Corps of Engineers*. Washington, DC 20314 – 1000
37. Yakut H, Tabar E, Yıldırım E, Zenginerler Z, Ertugral F, Demirci N (2016) Soil Gas Radon measurement Around Fault Lines On The Western Section Of The North Anatolian Fault Zone In Turkey. Radiat Prot Dosimetry. 173(4):405–413
38. Northern Marmara Highway (KMO) Project Overview. General Directorate of Highways adapted from NMH website, last accessed on 01.11.2024
39. Leroueil S, Tavenas F. Pitfalls of back-analyses. Proc. 10th ICSMFE (Stockholm). 1981;1:185–190 https://www.issmge.org/uploads/publications/1/35/1981_01_0031.pdf

Publisher's Note

Springer Nature remains neutral with regard to jurisdictional claims in published maps and institutional affiliations.